

Positioning errors and efficiency in fiber spectrographs

Peter R. Newman

Apache Point Observatory, P.O. Box 59, Sunspot, NM 88349-0059; and Department of Astronomy, New Mexico State University, P.O. Box 30001, Las Cruces, NM 88003-8001

prn@apo.nmsu.edu

ABSTRACT

The use of wide-field multi-object fiber-input spectrographs for large redshift surveys introduces the possibility of variations in the observed signal-to-noise ratio across the survey area due to errors in positioning the fibers with respect to the target image positions, leading to position-dependent errors in the survey catalog. This paper brings together a comprehensive description of the sources of fiber-to-image position errors in different instrument designs, and quantifies their effects on the efficiency with which signal is recorded. For point sources, a function relating a fractional efficiency and an equivalent aperture correction to the fiber-to-image position error, the fiber diameter and the image size is plotted for typical values of fiber and image sizes found in current instruments. The tools required by observers to maximize the efficiency of fiber-spectrographic surveys are discussed.

Subject headings: instrumentation: spectrographs — techniques: spectroscopic — surveys — astrometry

1. Introduction

The SDSS (York et al. 2000) and 2dF surveys (Boyle et al. 2001) exemplify the deep, wide-field redshift surveys now being conducted. These surveys aim to produce homogeneous three-dimensional maps of $\sim 3 \times 10^5$ to 10^6 extragalactic objects to $B \simeq 21$, about 10 per cent of which will be quasars. Such surveys rely on multiplexed instruments to record spectra at rates of thousands of candidates per night. The multi-object optical fiber-input spectrographs being used for the 2dF and SDSS surveys represent a culmination of more than two decades of instrument development, during which time more than 35 fiber spectrographs have been built or proposed, and more of which can be expected in the future.

Constructing catalogs from such large observational data sets requires automated analysis if reliable and consistent spectral classifications and redshift measurements are to be achieved. The probability of correct results from automated analysis depends primarily on the signal-to-noise ratio (SNR) of the reduced spectra, and the SNR is strongly affected by how much of each target

image actually falls on a spectrograph aperture. With single-object spectrographs, it is common practice to adjust telescope pointing during each exposure to maximize the signal recorded. While difficult to achieve to any degree with multi-object instruments, such adjustments, at best, result in an optimal *mean* signal, averaged over all the apertures. Offsets between the fiber and image positions during exposure will clearly reduce the recorded signal for all types of observed object. However, while typical galaxy images are $\gtrsim 3$ arcsec across at all redshifts (for a Hubble constant of $75 \text{ km s}^{-1} \text{ Mpc}^{-1}$), giving some natural tolerance to fiber positioning errors, quasar images are usually seeing-limited at $\sim 0.5\text{--}2.0$ arcsec diameter and thus demand greater precision in positioning each fiber.

Where a survey is constructed from the consolidation of tiled multi-object spectrograph observations, each exposure will be made under different conditions, leading to variations in the rate at which signal is recorded. In addition to random variations in fiber position errors, the errors may vary systematically across each tile leading to position-dependent selection effects that repeat from field to field. Survey catalogs may thus suffer from very complicated position-dependent measurement errors if the variations in SNR are left uncorrected, creating problems for the analysis of large-scale structure.

With perfect fiber positioning, telescope guidance, seeing conditions, and sufficiently wide fibers, essentially all of the incident image of an observational candidate will fall into the spectrograph input aperture. In practice, spectrograph designs are such that the optimum fiber diameter is a compromise influenced by factors that include the telescope focal ratio, the fiber acceptance angle, the expected seeing disk size and the desire to minimize contamination of the object spectra with sky light (Brodie, Lampton & Bowyer 1988), leaving many possible sources of loss of efficiency. Mismatches between the telescope beam, fiber aperture and the central obstruction in reflecting telescopes may lead to systematic losses (Wynne 1992). Fibers are mounted on surfaces that only approximate the true telescope focal surface and telecentric alignment. Atmospheric dispersion and differential refraction place strong constraints on fiber positioning (Donnelly et al. 1989) and the timing of observations. The accuracy of pointing and focus in modern telescopes is good, but still not perfect. All of these factors lead to the conclusion that, in practice, some offset of the each fiber from its target image is unavoidable.

How do these fiber positioning inaccuracies and other observational parameters affect the level of signal recorded? Hill (1993) gave a qualitative introduction to most of the issues involved, and Cuby (1994) addressed some of the issues quantitatively for the specific example of the VLT, but there has been little consolidation of the general problem in the literature. The aim of this paper, then, is to provide a comprehensive list of the sources of fiber position errors and to quantify their effects on efficiency when fiber spectrographs are used to observe point sources such as quasars. The rest of the paper is organized as follows. Section 2 defines the functions that measure the efficiency of spectrographic observations in terms of fiber position error. Section 3 describes the sources of position errors. Section 4 quantifies the efficiencies achievable for different fiber sizes, seeing conditions and fiber position errors. Finally, section 5 discusses the effects of the achieved

efficiencies on wide-field surveys and the requirements for software tools to aid in their efficient execution.

2. Efficiency of spectrographic observations

The efficiency of observation, η , for an individual object targeted by a spectrograph may be defined as the fraction of the total light in the object's image that actually enters the spectrograph input aperture during an exposure. For a planar aperture, this is given in general by

$$\eta = \frac{\int_{t_e} \int_{A(\mathbf{r})} \Omega_A dA dt}{\int_{t_e} \Omega_F dt} \quad (1)$$

where Ω_F is the intensity distribution of the image in the focal surface of the telescope, Ω_A is the intensity distribution of the image in the plane of the aperture, t_e is the exposure time, A is the aperture and \mathbf{r} is the separation vector from the center of the aperture to the center of the image in the plane of the aperture. \mathbf{r} , Ω_A and Ω_F will all vary with time. An aperture correction or equivalent loss in magnitudes may also be defined as $m_a = -2.5 \log(\eta)$.

The form of both Ω_F and Ω_A clearly depends on the nature of the objects being observed, the atmospheric seeing conditions and the telescope optical design. This paper considers point sources as a worst case because the effect on η of fiber position errors orthogonal to the optical axis will clearly be larger for point sources than for extended sources. The ideal point-spread function is the so-called Airy pattern (see for example Schroeder 1987, p. 180), but the detailed profile of the image of a point source after it has been convolved with telescope distortions, random motions from guiding errors and the effects of the atmosphere and then integrated over exposure times long enough to blur individual motions is, in practice, quite complex (King 1971; Woolf 1982). However, for the purposes of this paper both Ω_F and Ω_A for a point source image are adequately modelled by a 2-dimensional Gaussian with circular cross-section and known full width at half maximum (FWHM), W , given by

$$\Omega(\rho, \sigma) = \frac{1}{2\pi\sigma^2} \exp\left[\frac{-\rho^2}{2\sigma^2}\right] \quad (2)$$

where ρ is the radial position with respect to the center of the image, $\sigma = W/2\sqrt{\ln 4}$, which may be expected to vary with time, and the constant factor normalizes $\int_0^\infty \Omega d\rho = 1$.

It is well known that the atmosphere disperses the image of a point source into a short spectrum (Filippenko 1982), so an important proviso to the use of this simple form of Ω is that the integrals are only applicable to a *single wavelength* for all observations away from the zenith in the absence of atmospheric dispersion compensation. Chromatic aberration in the telescope optics has similar wavelength-dependent effects on Ω . The problem atmospheric dispersion raises for spectrophotometry is not treated further here (for a comprehensive analysis, see Donnelly et al. 1989) but the related effects of atmospheric dispersion on *guiding* and differential atmospheric refraction across

the telescope field are addressed in §3.1.7 and §3.1.8. Although Eqn.1 applies to any aperture, this paper deals with fibers which are modelled as simple circular apertures of diameter d .

3. Sources of position errors

The total position error for a fiber, \mathbf{r} , may be defined as the vector from the center of the physical fiber entrance aperture to the center of its target objects' image on the telescope focal surface, so $\mathbf{r} = 0$ indicates an image centered and focused on the fiber entrance aperture. The magnitude of \mathbf{r} can be resolved into its projection onto the focal surface, r_n , which moves the fiber on a plane orthogonal to the optical axis, and its projection onto the optical axis, r_p , which moves the fiber in a direction parallel to the optical axis. In addition, the alignment between the axis of the fiber at its entrance aperture and the incident telescope beam must be considered.

Sources of orthogonal, parallel and alignment angle errors will now be described in the approximate order in which each is introduced into observations. Orthogonal errors are measured either by linear offsets across the focal surface or by angular offsets across the sky. Parallel errors are measured by linear offsets along the telescope axis. Alignment errors are measured by the telecentric angle, θ_T (i.e. the angle between the fiber axis and the central ray of the telescope beam to the fiber). Parameters used are f , the telescope focal ratio; p , the mean telescope image scale in the sense of angular separation on the sky per unit linear separation on the focal surface; δr , the contribution to a linear offset from one source of error; θ , the total angular displacement on the sky; $\delta\theta$, the contribution to θ from one source of error; W_F , the FWHM of a point-source image on the telescope focal surface; and W_A , the FWHM of the image of a point source measured at the fiber entrance aperture. Airmass is measured by $\sec z$, where z is the angular separation of a point on the sky from the zenith. Unless otherwise noted, each source of error is independent of the others. Orthogonal errors may thus be combined as $\theta^2 = (r_n p)^2 = \sum(\delta\theta)^2 = \sum(\delta r_n p)^2$, and parallel errors combined as $r_p^2 = \sum(\delta r_p)^2$.

3.1. Errors orthogonal to the optical axis

3.1.1. Astrometry

The first source of orthogonal error comes from the astrometry in the target input catalog. It is easy to suppose that recent all-sky astrometric catalogs should make it is simple to achieve r.m.s. astrometric errors $\delta\theta \ll 1$ arcsec over wide fields, but this is not necessarily the case. First, astrometric catalogs such as the USNO-A2.0 (Monet et al. 1998) that combine faint magnitudes and all-sky coverage have in general been derived from measurements of single-epoch or averaged-epoch photographic survey plates with ages of up to 50 years or more, introducing large and variable proper motion uncertainties to positions at the current epoch.

Even with astrometric catalogs that include good proper-motion data, such as Tycho-2 (Høg et al. 2000), many other factors must be taken into account to achieve accurate calibration of target positions. The next requirement is that the centroids of the astrometric standard stars and the target objects are found in the source material to good precision and in the same reference frame. This is not trivial when wide magnitude ranges are covered, particularly for target catalogs based on photographic plates or that rely on brighter astrometric catalogs, as the reference stars may be saturated or comatic in deep source material. Tycho-2, for example is complete at the 95 per cent level only to $V \simeq 11.5$, still much brighter than the guide stars and targets typical of fiber spectroscopy. The forthcoming USNO-B catalog (Monet 2000) and the second-generation Guide Star Catalog (Morrison & McLean 2001) which will combine all-sky coverage, high-precision positions to faint magnitudes and accurate proper motions promise to be of great use for fiber spectroscopy.

Target positions derived from wide-field photographic plates may also include magnitude-dependent systematic errors of $\delta\theta \simeq 0.05 \text{ arcsec mag}^{-1}$ (Lu et al. 1998). Atmospheric dispersion can introduce a color-dependent shift in apparent positions in any source material as it does in spectrographic observations (§3.1.7), so it is important to match the filters used for the source material to the wavelengths for which spectra are to be obtained or to apply an appropriate correction.

Where the input catalog is derived from tiled observations, for example from adjacent photographic survey plates, great care (see for example Taff, Lattanzi & Bucciarelli 1990) must be taken at the boundaries between plates to avoid steep local gradients or step inhomogeneities in the spatial distribution of astrometric errors in a target catalog which may otherwise have a small mean error on the scale of each spectrographic field (Newman 1999). Similar care is needed when the astrometric calibration catalog is broken into separate zones, as with the Guide Star Catalog (Russell et al. 1990), or at the boundaries of the surveys from which the astrometric catalog was constructed. The USNO-A2.0 catalog, for example, has been shown to include discontinuities of $\sim 0.3 \text{ arcsec}$ at the boundary between the northern and southern Schmidt surveys from which it was built (Assafin et al. 2001).

Note that a first-order *systematic* astrometric error that shifts all fibers by the same vector is easily removed when the guide stars are centered in their fibers during observations, provided the guide star positions are in the same astrometric system as the target object positions. If the fiber mount plate can be rotated on the telescope, then a systematic rotation (such as that from precession) can also be easily removed.

3.1.2. *Aberration, parallax and proper motion*

The motion of an observer relative to an observed object produces a tilt of the apparent direction of the object toward the direction of motion of the observer due to the finite speed of light. This tilt is known as stellar aberration, or often simply aberration. The magnitude of the

tilt depends on the relative velocity and the angle, Θ_a , between the directions of observation and motion. The full correction naturally involves the special theory of relativity, but for terrestrial observations, the change in apparent position of an object due to the Earth’s motion about the Sun is well approximated by

$$\begin{aligned}\Delta\alpha &= \frac{-k}{\cos\delta}(\sin\Lambda\sin\alpha + \cos\Lambda\cos\epsilon\cos\alpha) \\ \Delta\delta &= -k\sin\Lambda\cos\alpha\sin\delta \\ &\quad +k\cos\Lambda(\cos\epsilon\sin\alpha\sin\delta - \sin\epsilon\cos\delta)\end{aligned}\tag{3}$$

where $k = 20.496$ arcsec is the constant of aberration for the Earth’s orbital motion about the Sun, (α, δ) are the true right ascension and declination of the object, Λ is the true solar longitude, ϵ is the obliquity of the ecliptic, and $(\Delta\alpha, \Delta\delta)$ are the change in apparent position in the sense apparent coordinate minus true coordinate (Lang 1986, and references therein).

Annual aberration due to the Earth’s orbital motion about the Sun ranges from $\Delta\Theta_a = 0$ for $\Theta_a = 0^\circ$ to $\Delta\Theta_a = 20.47$ arcsec for $\Theta_a = 90^\circ$, so the mean *differential* annual aberration across a telescope field is $20.47/90 \simeq 0.23$ arcsec deg $^{-1}$ in the sense that the field is compressed in the direction parallel to the Earth’s motion. The annual aberration at the planned time of observation should therefore be included when deriving fiber positions to remove this differential displacement across the telescope field. The maximum diurnal aberration due to the rotation of the Earth is ~ 0.32 arcsec, so the mean differential diurnal aberration is ~ 0.004 arcsec deg $^{-1}$ and may therefore be neglected.

Because aberration depends on both Λ and Θ_a , the correction for annual aberration for a target field depends on the date of observation as well as the hour angle. For example, observing a 3° -wide equatorial field one lunation later than that for which the fiber positions were designed, under the circumstances in table 1, results in a change in field compression due to differential aberration of 0.24 arcsec. Assuming the field is centered on the mount plate in both cases, images at the edge of the field are therefore displaced by $\delta\theta = 0.12$ arcsec with respect to their nominal positions, with $\delta\theta$ for other fibers being proportional to their radial distance from the center of the field. This may be partially compensated for by adjusting the telescope image scale.

Parallax of guide stars (and nearby targets) should also be corrected for the time of observation, but this can be difficult when anonymous guide stars are used, as their parallax will be unknown. Similarly, proper motion of guide stars or nearby targets between the time of observation of the source material and the time of the spectrographic observations should be corrected, especially if the age of the source material is high, but again, this is only possible if the proper motions are known. However, using sufficient guide stars for each observed field should make the mean parallax and proper motion errors negligible. Choosing guide stars with hot spectral types will further reduce both the mean parallax and proper motion, because they will be at a greater distance than cooler stars for a given apparent magnitude. If the spectral types of guide stars are not known with precision, then using a single color, e.g. $(B - V)$ or $(U - B)$, to select guide stars with blue

colors may suffice, but as discussed in §3.1.7, it may be more important to match guide star colors to target object colors.

3.1.3. Conversion to focal-surface coordinates

Accurate conversion of apparent positions on the sky into focal surface coordinates depends on accurate mapping of the focal surface. Cudworth & Rees (1991) showed that it can be difficult to determine p for wide-field telescopes to better than 1 part in 10^4 and to determine the distortion coefficients that describe how p varies across the field of view to better than 1 part in 10^3 . An error in p of this scale at a field radius of 1° leads to position uncertainties of $\delta\theta = 0.36$ arcsec. Even where the distortion is well mapped, errors in defining the center of the distortion field alone will lead to systematic errors in fiber coordinates. In the case of the CTIO 4-m telescope Cudworth & Rees (1991) showed that a 1 mm error in defining the center of the distortion field leads to position errors of $\delta\theta \simeq 1.4$ arcsec at a 25 arcmin field radius. Because distortion from centering errors will in general be anisotropic, its effect cannot be fully removed by simply centering the guide stars and adjusting the mean image scale.

Any lateral chromatic aberration in the telescope optical design will vary the distortion pattern by moving the center of Ω_F orthogonal to the optical axis for each wavelength, spreading each image radially with respect to the center of the focal surface. This wavelength dependence should be included when designing plate coordinates, unless the optical design provides good correction. In the case of the 2dF, the 4-element corrector design leaves a residual variation of < 1 arcsec over the full range of spectrographic wavelengths (Lewis et al. 2002), significantly less than W_F .

In drilled-plate systems, the bending of the fiber mount plate required to match the telescope focal surface (§3.2.1) will also introduce a change in the position of the fiber mounting holes orthogonal to the optical axis. In the SDSS case, for example, this amounts to $\sim 75 \mu\text{m}$ at the edge of the plates, which must also be corrected in the plate design.

Note that there are also separate problems introduced by temporal variations in mean p (§3.1.5) and imperfect optical collimation (§3.1.6).

3.1.4. Fiber mounting

The next source of orthogonal error comes from the mechanical positioning of the fibers on a mounting plate that is fixed in or subsequently moved to the telescope’s focus. Most fiber spectrographs use blind positioning of the fibers on a mount plate, where each fiber is positioned without reference to the actual positions of the target object images during observation. Coherent fiber bundles to image guide stars are positioned in the same way. The fibers are attached to the mount plate either directly, by fixing a fiber-carrying “puck” to the plate with a magnet or glue,

or by drilling holes in the plate into which ferrules, each carrying a centered fiber or fiber bundle, are plugged. A robot positions the fiber puck or a drill bit. Where a single (x, y) robot arm is used to position many pucks or holes, the robot typically has $\delta r_n \simeq 10\text{--}15 \mu\text{m}$ precision.

There have been several significant exceptions to the blind positioning approach. The Argus type of design (Ingerson 1993) uses individual robot arms for each fiber arranged as “anglers around a pond” at the periphery of the mount plate. This approach increases the speed with which a set of fibers may be positioned at the cost of increasing mechanical complexity. Argus itself cleverly allows for active fiber positioning in which fast sampling of a large synthetic aperture over each target image is used to find the actual centroid of the target and then make fine adjustments to the fiber positions¹, achieving residual radial position errors of $\delta\theta \simeq 0.2 \text{ arcsec}$, but offering the possibility of frequent correction to all other sources of error (Lutz et al. 1990). The FLAIR (Watson & Parker 1994) and MOFOCS (Pettersson 1988) designs position fibers using a human robot: the observing astronomer glues the pucks directly onto the images of targets on a copy of a photographic plate taken with the same Schmidt telescope used for spectroscopy, using a travelling microscope to position each fiber over the image of its target object. This method avoids the need to transform coordinates from the source material, and may be cheap to implement, but will introduce additional random and systematic errors that vary from plate to plate. Pettersson (1988) estimates this introduces errors $\delta r_n \lesssim 10 \mu\text{m}$, but the actual value will be difficult to measure and will no doubt vary between astronomers and with individual fatigue (Parker & Watson 1998). In addition, unless the spectra are observed under the same circumstances as the original plate was exposed, no corrections will be applied for aberration, parallax, proper motion, atmospheric dispersion or refraction.

A further source of orthogonal fiber mounting error comes from the centering of the fibers in their carrier pucks or ferrules. Minimizing these errors demands strict manufacturing controls, especially for cartridge-based instruments such as the SDSS spectrograph, for which ~ 6000 fibers have been fabricated. For all plug-plate instruments the subsequent centering of the ferrules in the plug-plate holes is also critical, as there must be a balance between the requirement that differences between the diameters of the ferrules and the plug-plate holes be small enough to ensure concentricity, but large enough to allow actual insertion and removal of the ferrule (Siegmund et al. 1998). Typical r.m.s. radial errors for the SDSS fibers, for example, are $\delta r_n \simeq 9 \mu\text{m}$ for the fiber-ferrule concentricity and $\delta r_n \simeq 8 \mu\text{m}$ for the ferrule-hole concentricity (Russell Owen, private communication, 2001).

¹Of course, this only works when the centroid of the image is the desired target.

3.1.5. Temporal variation in image scale

The fiber mount plate in most cases is metal and thus has a significant thermal coefficient of expansion, so corrections should be applied when the mount-plate coordinates are determined to compensate for the expected difference in temperature between the time the plate is drilled or the fiber pucks are placed and the time of observation. Any residual difference between the design and actual temperatures will introduce orthogonal position errors. Changes in the temperature of the telescope may also affect the image scale by moving the focal surface with respect to the primary mirror due to expansion or contraction of the telescope structure. These errors will be systematic and proportional to the radial distance of each fiber from the center of guiding.

This problem is more acute for instruments using pre-drilled plates because the time between positioning and observation will usually be much longer than for puck-positioning instruments, making it harder to predict the temperature at observation. The aluminum alloys typically used for pre-drilled plates have a higher coefficient of expansion ($\sim 25 \times 10^{-6} \text{ K}^{-1}$) than the steel used for magnetic-puck instruments ($\sim 12 \times 10^{-6} \text{ K}^{-1}$) or the glass used for glued-puck instruments ($\lesssim 10 \times 10^{-6} \text{ K}^{-1}$). For surveys using many plug plates, this problem is further exacerbated by the difficulties of scheduling when each plate is actually observed. Experience on the SDSS shows that the extreme design-to-observation difference in temperature may be as large as $\sim 20 \text{ K}$ for a plate repeatedly observed over a wide range of dates, resulting in scale differences of $\Delta p/p \simeq 5 \times 10^{-4}$. At the outside of the 328 mm-radius SDSS plug plates, this gives $\delta r_n \simeq 165 \text{ } \mu\text{m}$ equivalent to $\delta\theta \simeq 2.7 \text{ arcsec}$. In contrast, robotic puck-positioning instruments such as the 2dF have the advantage of positioning the fibers as late as $\sim 1 \text{ hr}$ before observation onto a plate that is already close to the observation temperature, so except at the start of each night when the rate of change of temperature may be large, the temperature difference between the time of plugging and the time of observation is unlikely to $\gtrsim 2\text{--}3 \text{ K}$. In the case of the 2dF, this difference has been found to be small and quite predictable although as yet uncorrected (Lewis et al. 2002).

There are generally two options available to compensate for residual image scale errors at the time of observation for puck and plug-plate instruments. The telescope may be defocused slightly, as this will often also change the effective image scale, but at the cost of a compromise between image scale and point-spread function size. This may be the only adjustment practical for instruments mounted at prime focus. Alternatively, in Cassegrain and other multiple-mirror systems, the position of the mount plate with respect to the primary mirror may be moved to change the effective focal length of the telescope and the secondary then moved to refocus. The SDSS telescope achieves this by moving the primary mirror along the optical axis, and is able to change its image scale by as much as $\Delta p/p \simeq \pm 5 \times 10^{-4}$ while still being able to achieve optimal focus. This permits the image scale error during exposures to be maintained to within a factor of $\Delta p/p \simeq \pm 2 \times 10^{-5}$ of optimal (equivalent to $\delta\theta = 0.1 \text{ arcsec}$ at the outside of its fiber mount plates) by applying scale corrections derived from automatic analysis of the observed positions of guide stars in their coherent fiber bundles. The mount for the Fruit & Fiber instrument on the du Pont 2.5m telescope at Las Campanas Observatory can similarly move with respect to the primary

by ~ 3 cm (Shectman 1993), allowing for a change of $\Delta p/p \simeq \pm 8 \times 10^{-5}$, although without the aid of automated analysis of scale error during observations.

3.1.6. Collimation and field rotation

Imperfect optical collimation introduces an optical distortion that remains static with respect to the optics, but which rotates during exposures with respect to the images, systematically moving the images with respect to the fibers. Good collimation is therefore particularly important in telescopes with alt-az mounts where there may be a large rotation of the field during each exposure. In the case of the SDSS telescope, this is expected to produce orthogonal errors $\delta r_n \lesssim 10 \mu\text{m}$ (Knapp et al. 1999) equivalent to $\delta\theta \lesssim 0.17$ arcsec. Because field rotation is much smaller on equatorially-mounted telescopes, instruments such as 2dF incur essentially zero variable error due to rotating distortion, but may still suffer from fixed-pattern errors if collimation is not perfect (§3.1.3).

3.1.7. Atmospheric dispersion and guiding

For a plane-parallel approximation of the atmosphere applicable at zenith angles typical of astronomy other than for solar observations near the horizon, the angle of refraction due to the atmosphere is given by

$$R(\lambda, z) = (n_\lambda - 1) \tan z \quad (4)$$

where n_λ is the refractive index of the atmosphere at wavelength λ relative to the vacuum and z is again the zenith angle (Green 1985). Filippenko (1982, and references therein) shows how n_λ varies with atmospheric conditions and how $R(\lambda, z)$ consequently varies with observing circumstances.

The first effect of $R(\lambda, z)$ on fiber positions comes from its dependence on λ , so that images of point sources observed away from the zenith are dispersed into short spectra orthogonal to the horizon, with the angular distance between two wavelengths $\delta\theta = R(\lambda_1, z) - R(\lambda_2, z)$. For example, at the center of the field under the designed observing circumstances in table 1, $\delta\theta \simeq 1.23$ arcsec. The effects of this atmospheric dispersion on spectrophotometric measurements with fiber spectrographs and the measures necessary to correct them are not treated here; for a comprehensive analysis, see Donnelly et al. (1989) and Filippenko (1982). However, fiber positions should be determined for a specific λ . This may be a common wavelength for all fibers, typically close to the central wavelength recorded by the spectrographs, or it may vary between target object types to record the most scientifically interesting regions of the target spectra.

Atmospheric dispersion must also be accounted for when there is a difference between the wavelength for which the fiber positions are designed and the apparent SED of the guide stars as recorded by the guide camera. This is particularly important when observing intrinsically-blue targets such as quasars, as most guide stars will have an apparent SED with a peak at a much longer

wavelength, which will therefore appear at a different initial offset within the dispersed images and see a different variation in offset with z . The problem is further increased because guiding normally tracks the brightest part of each guide star image, and the peak of the guide star SED varies from star to star and in any case is generally unknown. This problem may be reduced by filtering the guide camera. Refraction increases rapidly as λ decreases, so it is better to guide on the position of the red end of the dispersed guide-star images because a broad filter may then be used to admit sufficient light to the guide camera without incurring large differences between the position of the peak of the filtered guide star SED and the filter central wavelength for a variety of guide star SEDs. For example, guiding at $\sec z \leq 1.6$ through a filter with a central wavelength $\lambda_c = 6000 \text{ \AA}$ and a bandpass $\Delta\lambda = 2000 \text{ \AA}$ results in position errors of $\delta\theta \leq 0.05 \text{ arcsec}$ for guide stars with temperatures between 3000 K and 30000 K (Cuby 1994). An offset must then be applied between the guide and target fiber positions to place the optimum *observed* wavelength of the target spectra onto their fibers while tracking the filtered guide stars, but this offset increases the dependence of the fiber positions on the designed zenith angle.

It is theoretically possible to design an atmospheric dispersion compensator (ADC) by introducing prismatic elements into the optical path to cancel the effects of atmospheric dispersion without introducing other aberrations. The design and construction of precision ADC optics, as has been done for the 2dF spectrograph, is both complicated and costly (Lewis et al. 2002). In order to work at different airmasses, the prismatic elements must change their relative positions. This requires that they be collimated to very high precision or they will introduce further complications of image motion during long exposures (Willstrop 1987). Because of these complications, many fiber spectrographs dispense with ADCs and instead rely on larger fibers to collect the dispersed image.

3.1.8. Atmospheric differential refraction

The second effect of $R(\lambda, z)$ in Eqn. 4 comes from its dependence on z . For any non-zero field width, observations centered at $z = 0$ will be isotropically compressed by the difference in refraction between the zenith and the edge of the field. As the observation moves away from the zenith, the compression parallel to the horizon remains practically constant but that orthogonal to the horizon increases. For example, a 3° field at the designed circumstances in table 1 will be observed at $z = 35.7^\circ$ and compressed vertically by 3.5 arcsec at the central wavelength. When determining fiber mount-plate coordinates, a correction for $R(\lambda, z)$ must therefore be included, but problems arise if either the exposure is long enough for a significant change in airmass, or the actual observation is centered at an airmass significantly different from that for which the fiber positions were determined. If the same field is observed just 40 min late, then $z = 40.4^\circ$ and the field compression increases to 4.0 arcsec. Assuming the field is centered on the mount plate in both cases, images at the top and bottom edges of the field will be displaced by $\delta\theta = 0.25 \text{ arcsec}$ by an hour angle change of only 10° .

For fields at high altitude or designed for observation away from the meridian, a partial compensation for the change in field compression between the designed and observed z is possible by changing the image scale of the telescope by

$$\frac{\Delta p}{p} = \frac{(n_\lambda - 1)(\tan^2 z_{\text{des}} - \tan^2 z_{\text{obs}})}{2} \quad (5)$$

where z_{des} and z_{obs} are the designed and observed zenith angles, and the division by 2 equalizes the residual $\delta\theta$ error for a circular telescope field so that the movement of fibers towards the images perpendicular to the horizon is balanced by their movement away from the images parallel to the horizon. However, for fields at low altitude observed near the meridian, the limiting factor in determining the acceptable range of hour angles is the conflict between field rotation and fibers positioned for a central field compression, for which a combination of pointing, plate rotation and a scale change according to Eqn. 5 provides only partial correction. The uncorrected pattern will be a quadrupole with an amplitude proportional to the radial distance from the center of the plate.

3.1.9. Pointing and instrument rotation

The final source of orthogonal errors appears during the exposures. Random variations in telescope pointing about a constant mean position on the sky with variation time scales much shorter than the exposure time, when integrated over the exposure, will have the effect of convolving Ω_F with a Gaussian of width defined by the variance of the pointing errors. However, such pointing errors are *not* necessarily random in distribution and their correction will typically occur only a few times per minute depending on the integration time of the guide camera. Pointing errors may thus introduce a mean orthogonal fiber positioning error affecting all fibers equally. A reasonable expectation for modern automated guiding systems using multiple guide stars is that the r.m.s. error will be $\delta\theta \simeq 0.1$ arcsec.

A mean error in the fiber mount plate rotation angle, $\delta\Phi$, will introduce an orthogonal error $\delta\theta = pr\delta\Phi$ where r is the distance of the fiber from the center of rotation. However, this effect is generally very small. In the case of SDSS observations, for example, it is normal to maintain $\delta\Phi \lesssim 2$ arcsec, producing $\delta\theta \lesssim 0.05$ arcsec at the edge of the 328mm radius mount plates with an image scale $p = 16.5$ arcsec mm $^{-1}$.

3.2. Error parallel to the optical axis

3.2.1. Shape of the fiber mount plate

Without corrector optics, the focal surface of a telescope is unlikely to be close enough to a plane to permit the fiber mount plate to be planar without introducing significant variations in image quality across the field of view. In addition, the focal surface may vary with wavelength

due to longitudinal chromatic aberration in the telescope optics bringing different wavelengths to a focus at different positions parallel to the optical axis.

In principle, the fiber mount plate may be deformed when mounted on the telescope in order to bring all the fibers to the focus of the telescope beam, at least for some specific wavelength. The amount of distortion of the mount plate required to follow the focal surface depends on the optical design of the telescope and correctors and can vary quite widely between telescopes. For example, the sagittal depth (i.e. the depression of the center of the focal surface below the plane defined by the periphery of the field) of the SDSS telescope with the spectrographic corrector in place is 2.6 mm (Knapp et al. 1999), while that of the 2.5-m du Pont telescope is 7 mm (Shectman 1993). For drilled-plate systems, bending of the fiber mount plate is usually applied when the plate is attached to the telescope or installed in its cartridge, as in the Fruit & Fiber instrument, which distorts the plate by loading the edges of the plate with a pneumatic press, or the SDSS fiber cartridges, which use a combination of bolt-down edge loading and a central pull-down bar to achieve an acceptable profile. In practice, however, the deformed fiber mount plate is unlikely to follow the true shape of the focal surface, leading to defocusing errors which can vary also widely between instruments. The typical deviation of an SDSS fiber mount plate from the true focal surface measured at Apache Point Observatory when the plate is in the optimum position is $\delta r_p \simeq 80 \mu\text{m}$, which in an $f/5$ beam convolves Ω_F with a top-hat profile of diameter equivalent to $\sim 0.26 \text{ arcsec}$ on the sky. For the Fruit & Fiber spectrograph, the maximum deviation is typically $\delta r_p \simeq 1000 \mu\text{m}$ (Shectman 1993), equivalent to convolution of Ω_F with a top hat of $\sim 1.4 \text{ arcsec}$ diameter, leading to a very large variation in image sizes across the field.

For magnetic-puck instruments, the required distortion may be achieved by permanent bending of the mount plate, although this may complicate the requirements for the robotic positioner. Instead, the 2dF uses a corrector design that achieves a remarkably flat focal surface that is within $\delta r_p \leq 30 \mu\text{m}$ of planar across its entire field (Lewis et al. 2002). The maximum displacement is equivalent to the convolution of Ω_F with a top-hat profile of just 0.13 arcsec diameter, which is small compared to the mean seeing.

Further small parallel errors will result from fiber to fiber variations of the position of the fiber aperture with respect to the mounting surface of the ferrule or puck. Manufacturing tolerances can be expected to be of the same order as those for other ferrule dimensions, giving $\delta r_p \simeq 5 \mu\text{m}$. For plug-plate instruments there will be an additional and potentially larger variation in the actual seated position of the ferrule in the plug plate. Where the fibers are plugged into a mount plate already attached to the telescope, as with the Fruit & Fiber instrument, careful manipulation should ensure the seating error is negligible. However, experience has shown seating errors to be a problem for the SDSS plug-plate cartridges which are transported on a cart between the support building, where fibers are plugged into the mount plate, and the telescope. Vibration during this transport has on rare occasion caused a few fibers to fall completely out of their holes, and is thus likely to also move other fibers away from their fully-seated positions. At the time of writing, the resulting distribution of r_p is unknown, but it is suspected that holes near the periphery of the plates will

be less prone to errors than those near the center as the peripheral fiber carriers for those holes tend to be more tightly bent, thus putting larger torque on the ferrule-hole surface and so more firmly securing the ferrule. For instruments that glue pucks to the mount plate, variations in the thickness of the glue used to attach the fiber to the plate will vary r_p , but with careful application this also should be a matter of only a few microns. Magnetically-attached pucks should only incur the constant manufacturing error per puck, provided all mating surfaces are kept clean and free of corrosion.

3.2.2. *Focus errors during observation*

In Cassegrain systems, the secondary mirror position required to maintain focus will vary during observations due to changes in the temperature of the telescope and flexure in its structure. Similarly, the focal adjustment will vary with telescope temperature in prime-focus systems. Detecting focus variations requires a measurable image of the focal surface, typically from the coherent fiber bundles used to image the guide stars. Focus corrections are therefore subject to the same sampling and discreteness problems as guiding corrections (see §3.1.9), but also suffer from the additional problem that dynamic variations in the size of the true seeing disk, W_F , due to atmospheric changes may mask focus errors. Nevertheless, skilled observers should be able to maintain the images to within $(W_A - W_F) \simeq 0.2$ arcsec of best focus, equivalent to $\delta r_p = (W_A - W_F) f/p \mu\text{m}$. Systems to automate continuous focus adjustment may be possible if guide fibers can be displaced above and below the optimum focal surface to provide measures of differential focus. Note that corrections to focus are commonly accompanied by changes in image scale (see §3.1.5).

3.3. Sources of alignment error

Light may be lost between the exit aperture of the fibers and the dispersing element of the spectrograph if the axis of the fiber at its entrance aperture is not aligned with the central ray of the incident light beam in the so-called “telecentric” position (Wynne 1992, and references therein). This alignment may differ considerably from normals to the focal surface.

Drilled plug-plate systems offer a distinct advantage over puck-mounted fibers in this respect because the holes in the plug plate can be drilled to tilt all of the fibers close to $\theta_T = 0$ for any fiber arrangement. For example, in the SDSS spectrograph the telecentric angle of normals to the focal surface may be as large as $\theta_T \simeq 1.84^\circ$. The SDSS plates are deformed while being drilled such that when subsequently deformed (to a different shape) to follow the focal surface, the r.m.s. fiber alignment error is $\theta_T < 0.2^\circ$ (Siegmund et al. 1998). However, the bending during drilling introduces yet another radial displacement of the holes that must be corrected in the plate design.

Puck mounts, on the other hand, must be usable over a wide range of positions and orientations, and so must be designed to accept light at an angle to the usually flat mounting surface that is a

compromise to the variation in θ_T over the area each puck reaches, potentially resulting in larger losses. The 2dF mount plate, for example, has $0^\circ \lesssim \theta_T \lesssim 4^\circ$. Its pucks have a 2° offset built into their input prisms, leaving an uncorrected fiber alignment error of up to $\theta_T \simeq 2^\circ$ (Lewis et al. 2002), or ~ 13 per cent of the $f/3.5$ corrected input beam width.

4. Efficiencies and aperture corrections

Increasing r_n will decrease η for point sources because the fiber aperture will clearly be illuminated by a fainter region of the image². Increasing r_p for point sources will, in general, also decrease η because the defocused image illuminating the fiber aperture will have a lower surface brightness. The detailed transformation of Ω_F into Ω_A by defocusing depends on the nature of the telescope optical configuration, in particular the central obstruction in reflecting telescopes (Schroeder 1987) which eventually produces a classical “donut” image. The defocused image typically has complex structure from imperfections in the figures of the mirrors and their collimation, which may include bright spots. However, the effect of the small values of r_p that are likely during science exposures may be approximated to first order for point sources as a convolution of Ω_F with a top-hat of angular diameter $p r_p/f$. For practical purposes this may often be treated a simple increase in W_F by an additive term, giving the observed image FWHM at the aperture of $W_A \simeq W_F + (p r_p/f)$.

Figs. 1 and 2 show the fractional efficiency, η , and the equivalent loss in magnitudes, m_a , as a function of the total orthogonal error for a range of values of the total image FWHM measured at the fiber aperture. The orthogonal error and image FWHM are both expressed in fiber diameters, i.e. r_n/d and W_A/d , so the plots are applicable to all fiber spectrographs or indeed other spectrographs with circular apertures.

For a given survey, the actual orthogonal and parallel errors expected from each of the sources described above obviously depend upon many factors related to the sources of the target input catalog, the instrument and telescope design and the observational circumstances, so no attempt is made here to derive “typical” total values for r_n and W_A . However, once total values have been calculated for particular observational circumstances, Figs. 1 and 2 can be used to determine the fraction of the light that will enter the fiber targeted on each object and the corresponding aperture correction.

If fibers are not aligned in the telecentric position then η is reduced by a further factor. If u is the angular radius of the telescope beam, θ_T is the telecentric angle and B the fraction of the telescope beam that is unobstructed, then Wynne (1992) has shown that the proportional light loss

²For extended sources, increasing r_n may decrease or increase the total signal recorded, depending on the nature of the object being observed, but if it increases the signal, it will be the *wrong* signal coming from an part of the object other than the intended target.

factor is

$$\gamma = 1 - \frac{k\theta_T}{Bu} \quad (6)$$

where $k = 0.6$ is accurate to within a few per cent for $\theta_T/u \lesssim 1.4$. The net efficiency is then $\eta = \gamma\eta_0$ where η_0 is the efficiency arising from fiber position errors in the telecentric condition. Unless the spectrograph camera optics incorporate careful baffling after the fiber output, the lost light will become stray light in the spectrographs, further degrading the SNR.

5. Conclusions

This paper has quantified the principal factors that reduce the efficiency of observations made with fiber-input multi-object spectrographs. These include:

- Astrometry of the input catalog.
- Corrections for parallax and proper motion of guide stars.
- Corrections for annual aberration and atmospheric refraction.
- Optical collimation of the telescope and mapping of its image scale and distortion.
- Precision of the fiber positioning system.
- Curvature of the focal surface and the telecentric angle of the fibers.
- Differences between designed and actual observing circumstances.
- Precision of telescope pointing, instrument rotation and focus during integration.

Although small fibers may be desirable to reduce sky noise, Figs. 1 and 2 show that small fiber diameters place tremendous demands on fiber positioning precision. In the absence of ADC optics, small fibers also incur a heavier spectrophotometric penalty from atmospheric dispersion than larger fibers. Poor seeing, which may be defined as $W_F \gtrsim d$, greatly reduces the signal even from well-centered images. Systems to automate continuous focus adjustment may clearly improve efficiency by minimizing $(W_A - W_F)$.

Where tiled observations are used to construct a large survey, knowledge of the *distribution* of fiber position errors across each field is as important as knowing the mean error or else the survey may suffer from a very complicated position-dependent faint-object selection effects, or may show errors in spectral identification or redshift measurement correlated with position. In particular, when the fiber position error is proportional to the radial distance of the fiber from the field center because the telescope image scale is incorrect, the selection bias or spectral measurement errors may

echo the tessellation in the survey catalog. Removal of these effects for the analysis of large-scale structure requires very careful modelling.

The individual observations for large tiled surveys will typically be made under quite variable conditions. Even under photometric conditions, compensating changes to the exposure times used will be necessary when actual circumstances differ from those for which fiber positions were designed. Minimizing the effects of atmospheric refraction demands that fields be observed over a small range of airmass with exposures centered on the meridian, but this forces a compromise between correcting the compression of a field and its rotation during exposure. In practice, this constraint may cause great difficulties in scheduling observations around weather, particularly for instruments with fibers mounted well ahead of observation.

While extra exposures will not remove systematic differences in SNR across each tile, they can at least ensure that the required survey minima are achieved for an acceptable fraction of all objects. Nevertheless, additional observations beyond the design time for the fiber positions can leave strong *spectrophotometric* effects in the data as the atmospheric dispersion changes which must be corrected by other means, such as synthetic large-aperture spectra of bright stars of known spectral type obtained by moving the telescope about the mean pointing, from which an approximate spectrophotometric correction can be derived.

Given that the practical aspects of fiber positioning are fixed by the time the observations are made, what tools should observers have to maximize the efficiency of fiber spectrographic survey operations? The first tool required to compensate for variations in fiber-to-image position errors is accurate real-time evaluation of the actual SNR values recorded in an exposure. This will facilitate decisions as to how much additional exposure time is needed to achieve, but not excessively exceed, the required minimum SNR before fibers are reconfigured. In addition to all-fiber mean values, such tools should provide information on the spatial distribution of SNR across each field so that position-dependent systematics can be reduced. The SDSS observers at Apache Point Observatory have an excellent example of this in the form of a cut-down version of the full spectrographic reduction pipeline (Stoughton et al. 2002) known as Son of Spectro (SoS; David Schlegel & Scott Burles, private communications, 2001). SoS runs on a fast dual-processor computer on the mountain and provides SNR totals and distributions together with other quality assurance parameters within minutes of the end of each exposure, enabling timely decisions by the observers on what exposures are required to complete a field.

The importance of accurate and precise guiding in minimizing r_n and r_p demands a good auto-guiding system controlling all axes and other controls such as image scale and telescope focus. Efficient scheduling of observations with fiber spectrographs also requires a tool to help decide which field to observe next, in order to make best use of the available sky and conditions (for example, in avoiding moonlight). This is particularly true for surveys using plug-plates, where the queue of fields available each night must be specified well in advance, and each plate is only suitable for observations over a particular range of dates and airmasses. Again, the SDSS has a tool

built around the fiber mount plate database specifically for this purpose (Stephen Kent, private communications, 2002). This gives the observers up-to-date information on the plates available, the results of prior observations for the currently plugged plates, the sky brightness due to moonlight in the direction of each spectrographic field, and the optimum and allowable times of observation for each plate. Other factors not related to observational circumstances may also be included in such a tool, for example to record the scheduling priority assigned to each field when aiming to achieve timely contiguous coverage of large tiled areas.

Finally, it should be stressed that while the full extent of the problems of positioning fibers for efficient observation may seem daunting to new fiber-spectrographic observers, surveys such as the SDSS and 2dF that are relying on fiber spectrographs are achieving tremendous successes, clearly demonstrating that the problems can be adequately solved by attention to detail and the application of good engineering practice. The work required to achieve similar success in smaller scale observational programs with fiber spectrographs is just as difficult, so it is to be hoped that the tools developed for the large surveys will become available for broader use in due course.

I thank Terry Bridges, Russell Owen, and Jim Gunn for useful discussions, Steve Kent for a critical and very helpful review of a draft manuscript, and the anonymous referee for constructive comments.

REFERENCES

Assafin, M., Andrei, A.H., Vieira Martins, R., da Silva Neto, D.N., Camargo, J.I.B., Teixeira, R. & Benevides-Soares, P., 2001, *ApJ*, 552, 380

Boyle, B.J., et al., 2001, in *ASP Conf. Ser.* 232, *New Era of Wide Field Astronomy*, eds. Clowes, R., Adamson, A. & Bromage, G. (San Francisco: ASP), 65

Brodie, J.P., Lampton, M. & Bowyer, S., 1988, *AJ*, 96, 2005

Cuby, J.G., 1994, *Proc. SPIE*, 2198, 2

Cudworth, K.M. & Rees, R.F., 1991, *PASP*, 103, 470

Donnelly, R.H., Brodie, J.P., Bixler, J.V. & Hailey, C.J., 1989, *PASP*, 101, 1046

Filippenko, A.V., 1982, *PASP*, 94, 715

Green, R.M., 1985, *Spherical Astronomy* (Cambridge: CUP)

Hill, J.M., 1993, in *ASP Conf. Ser.* 37, *Fiber Optics in Astronomy II*, ed. Gray, P.M. (San Francisco: ASP), 235

Høg, E., et al., 2000, *A&A*, 355, L23

Ingerson, T.E., 1993, in *ASP Conf. Ser.* 37, *Fiber Optics in Astronomy II*, ed. Gray, P.M. (San Francisco: ASP), 76

King, I.R., 1971, *PASP*, 83, 199

Knapp, J., Gunn, J., Margon, B., Lupton, R. & Strauss, M., 1999, *The Sloan Digital Sky Survey Project Book*, available at <http://www.sdss.org/>

Lang, K.R., 1986, *Astrophysical Formulae*, 2nd ed. corrected (Berlin: Springer-Verlag)

Lewis, I.J., et al., 2002, preprint astro-ph/0202175

Lu, C.-L., Platais, I., Girard, T. M., Kozhurina-Platais, V., van Altena, W. F., López, C. E. & Monet, D. C., 1998, in *New Horizons from Multi-Wavelength Sky Surveys*, *Proc. IAU Symp.* 179, eds. McLean, B.J., et al. (Dordrecht: Kluwer), 384

Lutz, T.E., Ingerson, T., Schumacher, G. & Smith, D., 1990, *PASP*, 102, 1208

Monet, D., et al., 1998, *USNO-A V2.0 A Catalogue of Astrometric Standards* (Washington: U.S. Naval Observatory)

Monet, D.G., 2000, *BAAS*, 32(4), 113.06

Morrison, J.E. & McLean, B., 2001, *BAAS*, 33(3), 6.03

Newman, P.R., 1999, PhD thesis, University of Central Lancashire

Parker, Q.A. & Watson, F.G., 1998, in *ASP Conf. Ser. 152, Fiber Optics in Astronomy III*, eds. Arribas, S., Mediavilla, E. & Watson, F. (San Francisco: ASP), 80

Pettersson, B., 1988, in *ASP Conf. Ser. 3, Fiber Optics in Astronomy*, ed. Barden, S.C. (San Francisco: ASP), 133

Russell, J.L., Lasker, B.M., McLean, B.J., Sturch, C.R. & Jenkner, H., 1990, *AJ*, 99, 2059

Schroeder, D.J., 1987, *Astronomical Optics* (San Diego: Academic Press)

Shectman, S.A., 1993, in *ASP Conf. Ser. 37, Fiber Optics in Astronomy II*, ed. Gray, P.M. (San Francisco: ASP), 26

Siegmund, W.A., Owen, R.E., Granderson, J., Leger, R.F., Mannery, E.J., Waddell, P. & Hull C.J., 1998, in *ASP Conf. Ser. 152, Fiber Optics in Astronomy III*, eds. Arribas, S., Mediavilla, E. & Watson, F. (San Francisco: ASP), 92

Stoughton, C., et al., 2002, *AJ*, 123, 485

Taff, L.G., Lattanzi, M.G. & Bucciarelli, B., 1990, *ApJ*, 358, 359

Watson, F.G. & Parker Q.A., 1994, *Proc. SPIE*, 2198, 65

Willstrop, R.V., 1987, *MNRAS*, 225, 187

Woolf, N.J., 1982, *Ann. Rev. Astr. Astroph.*, 20, 367

Wynne, C.G., 1992, *Pure & Applied Optics*, 1, 185

York, D.G., et al., 2000, *AJ*, 120, 1579

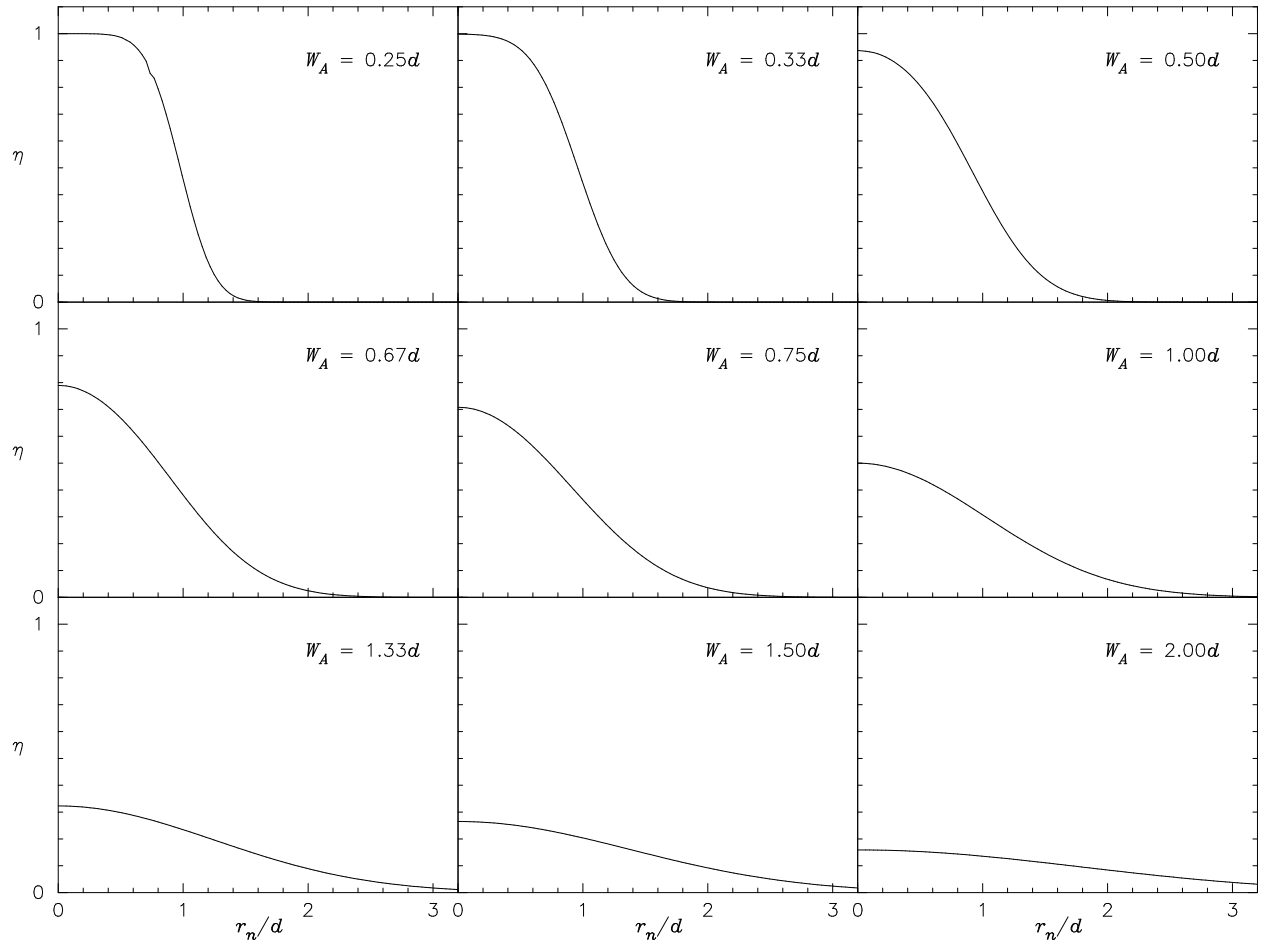


Fig. 1.— Fractional efficiency for point sources as a function of fiber-image displacement for a range of image sizes.

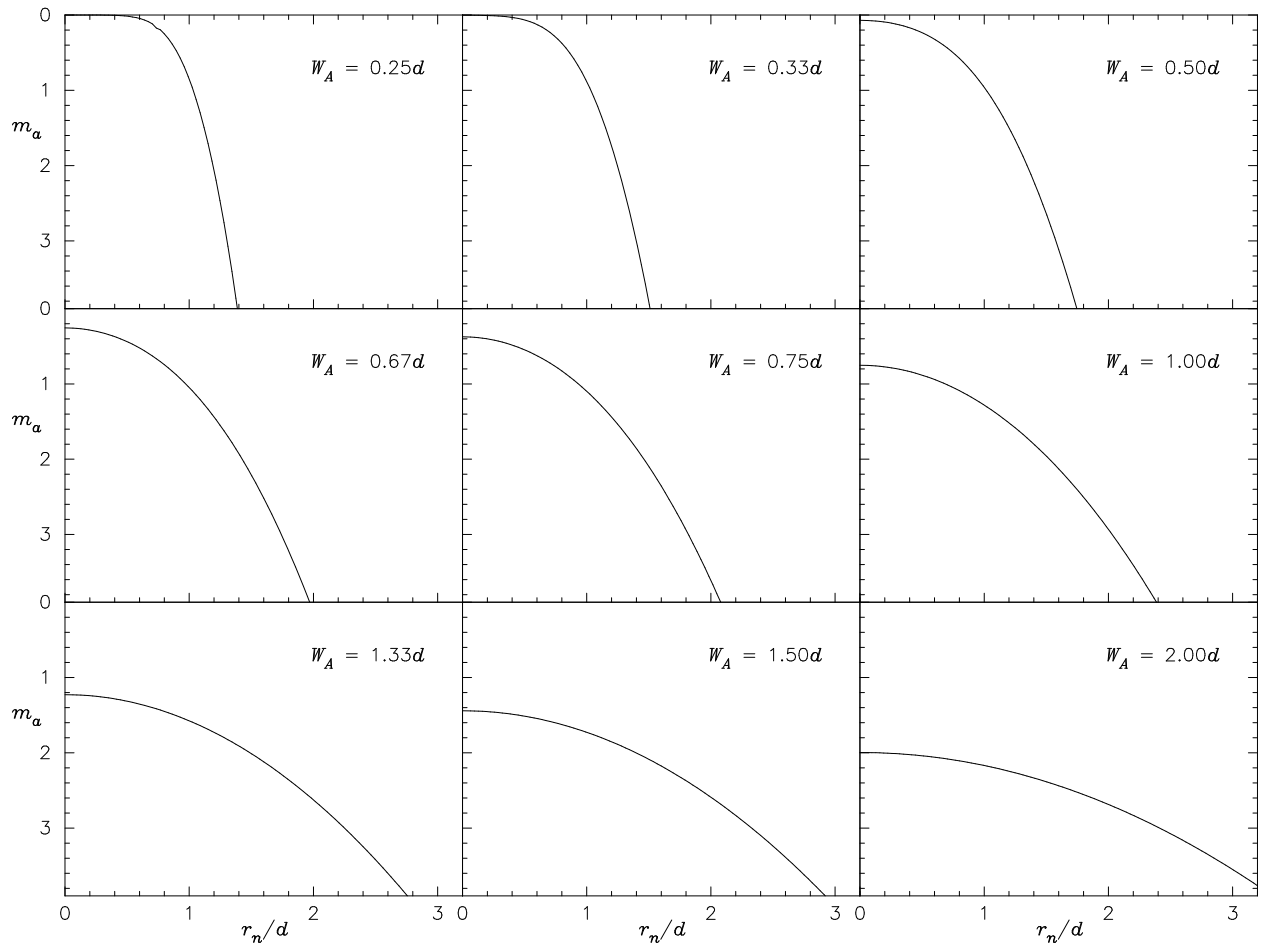


Fig. 2.— Efficiency for point sources expressed as an aperture correction in magnitudes for the same fiber-image displacements and image sizes shown in Fig. 1.

Table 1. Hypothetical observational circumstances used for examples, based on an equatorial field observed with the SDSS spectrographs with physical conditions typical of winter observing at Apache Point Observatory. The designed and actual dates of observation differ by one lunation.

Parameter	Actual	Designed
Telescope focal ratio f	5	
Field width	3°	
Image scale p	16.5 arcsec mm $^{-1}$	
Recorded wavelength range	3800–9200 Å	
Observatory altitude above sea level	2788 m	
Air pressure	550 mm Hg	
Ambient temperature	–4 C	
Relative humidity	40%	
Field center right ascension	0 ^h	
Field center declination	0°	
Central hour angle	25°	15°
Date of observation	2002 Feb 1	2002 Jan 3